Chemical Engineering Science 74 (2012) 135–147

Contents lists available at SciVerse ScienceDirect

Chemical Engineering Science

journal homepage: www.elsevier.com/locate/ces

Modeling and control of Transparent Conducting Oxide layer surface morphology for improved light trapping

Jianqiao Huang [a], Gerassimos Orkoulas [a], Panagiotis D. Christofides [a,b,*]

[a] Department of Chemical and Biomolecular Engineering, University of California, Los Angeles, CA 90095, USA
[b] Department of Electrical Engineering, University of California, Los Angeles, CA 90095, USA

ARTICLE INFO

Article history:
Received 19 January 2012
Received in revised form
16 February 2012
Accepted 21 February 2012
Available online 5 March 2012

Keywords:
Surface roughness
Visible light wavelength
Transparent Conducting Oxide (TCO) layer
Model predictive control
Distributed parameter systems
Thin film solar cells

ABSTRACT

This work first introduces a kinetic Monte–Carlo simulation model for a two species thin film deposition process and demonstrates the use of feedback control, coupled with a suitable actuator design, in manufacturing thin films whose surface morphology has a structure that improves light trapping. This work is relevant in the context of a Transparent Conducting Oxide (TCO) thin film layer manufacturing used in thin film solar cells where it is desirable to produce thin films with precisely tailored surface morphology. Specifically, a two species thin film deposition process involving atom adsorption, surface relaxation and surface migration is initially considered and is modeled using a large-lattice (lattice size=40,000) kinetic Monte–Carlo simulation. Subsequently, thin film surface morphology characteristics like roughness and slope are computed with respect to different characteristic length scales ranging from atomic to the ones corresponding to visible light wavelength and it is found that a patterned actuator design is needed to induce thin film surface roughness and slope at visible light wavelength spatial scales, that lead to desired thin film solar cell performance. Then, an Edwards–Wilkinson type equation is used to model the surface evolution at the visible light wavelength spatial scale and form the basis for the design of a predictive feedback controller whose objective is to manipulate the deposition rate across the spatial domain of the process. The model parameters of the Edwards–Wilkinson equation are estimated from kinetic Monte–Carlo simulations and their dependence on the deposition rate is used in the formulation of the predictive controller to predict the influence of the control action on the surface roughness and slope throughout the thin film growth process. Analytical solutions of the expected surface roughness and surface slope at the visible light wavelength spatial scale are obtained by solving the Edwards–Wilkinson equation and are used in the predictive controller formulation and in the control action calculation. The controller is applied to the large-lattice kinetic Monte–Carlo simulation. Simulation results demonstrate that the proposed controller and patterned actuator design successfully regulate aggregate surface roughness and slope to set-point values at the end of the deposition.

© 2012 Elsevier Ltd. All rights reserved.

1. Introduction

Thin film solar cells constitute an important and growing component of the overall solar cell market (see, for example, Green, 2007; van Sark et al., 2007) owing to the potential of improved light conversion efficiencies (currently on the order of 10% for production modules). The Transparent Conducting Oxide (TCO) layer, which typically consists of zinc oxide (ZnO) and aluminum (Al), is an important component of thin film solar cells and has a crucial influence on the performance of thin film solar cell systems (see, for example, Krč and Zeman, 2003; Gospodyn and Sit, 2006). In addition to investigating the performance with respect to light conversion efficiency and long-term stability of an array of materials, thin film solar cell technology stands to benefit from optimal thin film manufacturing (deposition) control strategies that produce thin films with desired light trapping properties. Specifically, extensive research on optical properties of thin-film TCO layers has demonstrated that the surface morphology at the interface, which is characterized by surface roughness and slope, directly influences the efficiency of thin-film silicon solar cells (see, for example, Gospodyn and Sit, 2006; Krč and Zeman, 2003; Zeman and Vanswaaij, 2000; Poruba et al., 2000; Muller and Rech, 2004; Rowlands et al., 2004). Shaping the surface morphology of the TCO layer at the thin film deposition stage is therefore critical in order to maximize the amount of light converted to electrical energy.

While developing accurate models for predicting optical properties of TCO thin films is an on-going research topic, it is

* Corresponding author at: Department of Chemical and Biomolecular Engineering, University of California, Los Angeles, CA 90095, USA. Tel.: +1 310 794 1015; fax: +1 310 206 4107.
E-mail address: pdc@seas.ucla.edu (P.D. Christofides).

0009-2509/$ - see front matter © 2012 Elsevier Ltd. All rights reserved.
doi:10.1016/j.ces.2012.02.030

well-established that the root-mean-square surface roughness and slope at characteristic length scales that are comparable to the wavelength of the visible light are key factors that influence thin film optical properties (e.g., Huang et al., 2011b; Krč and Zeman, 2003). Despite the importance of these efforts and the broad realization that the surface morphology of the TCO layer could be tailored to improve thin film solar cell efficiency, the problem of shaping the TCO thin film surface morphology during film deposition by appropriately controlling the surface slope and roughness to desired levels has received limited attention. Thus, it is desirable to develop systematic approaches to manufacture thin film solar cells with optimal light conversion efficiencies via computational multi-scale modeling and real-time model-based control of the manufacturing process.

Over the last 20 years within the control engineering literature, extensive efforts have been made on the modeling and model-based feedback control of thin film deposition processes with emphasis on the problems of film thickness, roughness and porosity regulation. Microscopic modeling of thin film growth is usually carried out via kinetic Monte–Carlo (kMC) methods (see, for example, Gillespie, 1976; Reese et al., 2001; Christofides et al., 2008 for results and references in this area) as well as stochastic partial differential equations (e.g., Edwards and Wilkinson, 1982; Vvedensky et al., 1993; Lauritsen et al., 1996). With respect to model-based feedback control of thin film deposition, early efforts focused on deposition spatial uniformity control on the basis of continuum-type distributed parameter models (e.g., Christofides, 2001), while within the last 10 years, most attention has focused on control of thin film surface morphology and microstructure. Since kMC models are not available in closed form and cannot be readily used for feedback control design and system-level analysis, stochastic differential equation (SDE) models (whose parameters are computed from kMC model data) have been used as the basis for the design of feedback controllers to regulate thin film surface roughness (e.g., Christofides et al., 2008; Ni and Christofides, 2005; Varshney and Armaou, 2005, 2006; Hu et al., 2009a), film porosity (Hu et al., 2009a,b), and film thickness. In an attempt to manufacture thin film solar cells with optimal light conversion efficiencies, we previously conducted research on the modeling and control of silicon thin film surface morphology to optimize thin film light trapping properties (Huang et al., 2011b, 2012), both at the atomic level and at an aggregated level comparable to the visible light wavelength (Huang et al., 2011b; Zhang et al., 2012).

Motivated by the above considerations, in the present paper, we focus on the application of microscopic modeling and control to the process of TCO thin film deposition, which consists of ZnO and Al. Specifically, this work introduces a two species simulation for TCO layer deposition process and presents an integrated control actuator and control algorithm design framework for the regulation of deposition of TCO thin films such that the final thin film surface morphology is controlled to a desired level. To demonstrate the approach, we focus on a two species thin film deposition process using a large-lattice (lattice size = 40,000) kinetic Monte–Carlo simulation. Different deposition mechanisms are utilized for each component, ZnO and Al. Specifically, random deposition with surface relaxation (RDSR) mechanism is used for Al and deposition/migration mechanism is used for ZnO (Huang et al., 2010). Subsequently, surface roughness and slope at different length-scales ranging from atomic scale to visible light wavelength scale are both calculated based on the generated thin film surface. It is found that a patterned actuator design is needed to induce thin film surface roughness and slope at visible light wavelength spatial scales to desired levels. Since a large-lattice kinetic Monte–Carlo model cannot be used as the basis for controller design and real-time controller calculations, an Edwards–Wilkinson type equation is used to model the surface evolution at the visible light wavelength spatial scale and to form the basis for feedback controller design within a model predictive control framework. The cost function of the predicted controller involves penalties on both surface roughness and slope from set-point values as well as constraints on the magnitude and rate of change of the control action. The Edwards–Wilkinson equation model parameters are estimated from kinetic Monte–Carlo simulations and their dependence on the manipulated input (deposition rate) is used to predict the influence of the control action on the surface roughness and slope during the growth process. The controller formulation takes advantage of analytical solutions of the expected surface roughness and surface slope at the visible light wavelength spatial scale and the controller is applied to the large-lattice kinetic Monte–Carlo simulation. Extensive simulation studies demonstrate that the proposed controller and patterned actuator design successfully regulate surface roughness and slope at visible light wavelength spatial scales to set-point values at the end of the deposition.

2. Two species thin film deposition process description and modeling

In this section, a one-dimensional solid-on-solid (SOS) on-lattice kinetic Monte–Carlo (kMC) model is used to simulate the two species thin film deposition process, which includes three microscopic processes: an adsorption process, in which particles are incorporated into the film from the gas phase, a migration process and a surface relaxation process, in which surface particles move to adjacent sites (Levine et al., 1998; Levine and Clancy, 2000; Wang and Clancy, 2001; Yang et al., 1997). The model is valid for temperatures $T < 0.5T_m$, where T_m is the melting point of the deposited material (Levine et al., 1998). At high temperatures ($0.5T_m \lesssim T \lesssim T_m$), the particles cannot be assumed to be constrained on the lattice sites and the on-lattice model may not be valid. In this work, a square lattice is selected to represent the structure of the film, as shown in Fig. 1. All particles are modeled as identical hard spheres and the centers of the particles deposited on the film are located on the lattice sites. The diameter of the particles equals the distance between two neighboring sites. The width of the lattice is fixed so that the lattice contains a fixed number of sites in the lateral direction. The new particles are always deposited from the top side of the lattice with vertical incidence; see Fig. 1. Particle deposition results in film growth in the direction normal to the lateral direction. The direction normal to the lateral direction is thus designated as the growth direction. The number of sites in the lateral direction is defined as the lattice size and is denoted by L. Periodic boundary conditions (PBCs) are applied at the edges of the lattice in the lateral direction.

The top particles of each column are defined as the surface particles and the positions of the centers of all surface particles form the surface height profile. The number of nearest neighbors of a surface particle ranges from zero to two. A surface particle with zero nearest neighbors is possible to move to one of its adjacent columns with equal probability. A surface particle with one nearest neighbor is possible to move to its adjacent column with lower height. A surface particle with two nearest neighbors cannot move. Particles that are not on the film surface cannot move.

The overall deposition rate, w, is expressed in the unit of layer per second and is a combination of two components, ZnO deposition rate w_1 and Al deposition rate w_2 ($w = w_1 + w_2$). The deposition ratio between ZnO and Al is 24:1 (Das et al., 2005). Different deposition mechanisms are used for each component. Random deposition with surface relaxation (RDSR) mechanism is used for Al. Specifically, in the RDSR process a site is randomly selected with uniform probability among all lattice sites and a particle is deposited on the top of this site. If the just deposited particle has less than two nearest neighbors, it will move according to the rules described above. A deposition/migration mechanism is used for ZnO. In this model, the

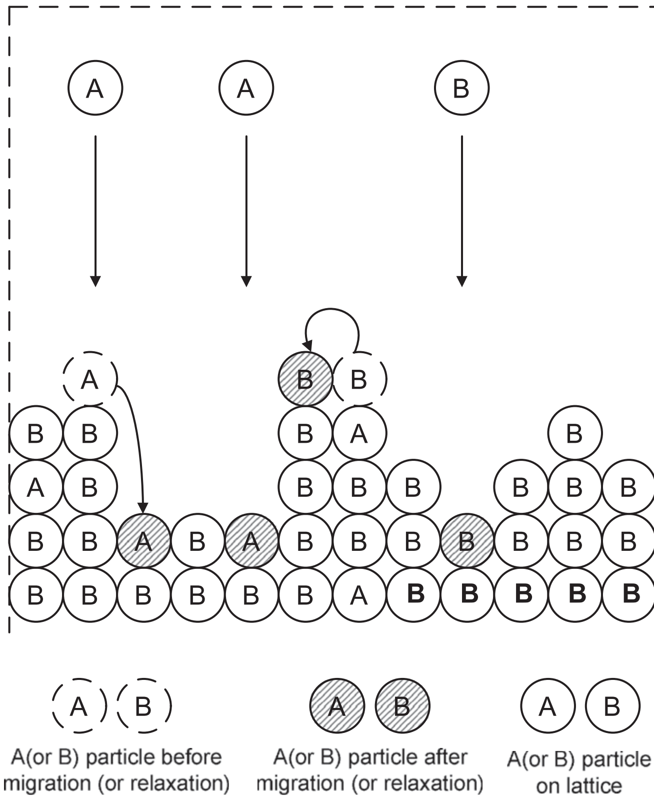

Fig. 1. Two species thin film growth process on a solid-on-solid one-dimensional square lattice.

deposition and migration events are separate and independent microscopic events. The deposition event is a random process, i.e., the same random deposition (without surface relaxation) as in the RDSR model. However, the migration event does not follow immediately the deposition of the particle. Instead, each surface particle, i.e., the top particle of a lattice site, is subject to its own migration event with a probability that depends on its local environment and the substrate temperature. The migration rate (probability) follows an Arrhenius-type law with a pre-calculated activation energy barrier that depends on the local environment of the particle, i.e., the number of the nearest neighbors of the particle chosen for a migration event. The migration rate of the ith surface particle is calculated as follows:

$$r_m = v_0 \exp\left(-\frac{E_s + n_i E_n}{k_B T}\right) \tag{1}$$

where v_0 denotes the pre-exponential factor, n_i is the number of the nearest neighbors of the ith particle and can take the values of 0 and 1, (r_m is zero when n_i=2 since in the one-dimensional lattice this surface particle is fully surrounded by other particles and cannot migrate), k_B is the Boltzmann's constant, E_s is the contribution to the activation energy barrier from the site itself, and E_n is the contribution to the activation energy barrier from each nearest neighbor. In this work, $E_s = 3.4$ eV and E_n is assumed to be zero (Moller and Palumbo, 2001). T is the substrate temperature of the thin film and in this work T=800 K (Mirica et al., 2004). Since the film is thin, the temperature is assumed to be uniform throughout the film. For the detailed description and investigation of these models, refer to Huang et al. (2010).

2.1. Surface morphology at atomic level

Thin film surface morphology, which can be expressed in terms of surface roughness and slope, is a very important surface property influencing the light properties of TCO thin films. Surface roughness is defined as the root-mean-square (RMS) of the surface height profile. Specifically, the definition of surface roughness is given as follows:

$$r = \left[\frac{1}{L}\sum_{i=1}^{L}(h_i - \overline{h})^2\right]^{1/2} \tag{2}$$

where r denotes surface roughness, h_i, $i = 1, 2, \ldots, L$, is the surface height at the i-th position in the unit of layer, L denotes the lattice size, and the surface mean height is given by $\overline{h} = (1/L)\sum_{i=1}^{L} h_i$.

In addition to surface roughness, another quantity that also determines the surface morphology is the surface mean slope. In this work, the surface mean slope is defined as the RMS of the surface gradient profile as follows:

$$m = \left[\frac{1}{L}\sum_{i=1}^{L} h_{s,i}^2\right]^{1/2} \tag{3}$$

where m denotes the RMS slope and $h_{s,i}$ is the surface slope at the i-th lattice site, which is a dimensionless variable. The surface slope, $h_{s,i}$ is computed as follows:

$$h_{s,i} = \frac{h_{i+1} - h_i}{1} \tag{4}$$

Since the unit of height is layer and the distance between two adjacent particles (the diameter of particles) always equals to one layer, the denominator of $h_{s,i}$ is always one. Due to the use of PBCs, the slope at the boundary lattice site (i=L) is computed as the slope between the last lattice site (h_L) and the first lattice site (h_1).

To investigate the open-loop properties of surface morphology, a set of kMC simulations is carried out at different w with T=800 K and L=40,000. In particular, the continuous-time Monte–Carlo (CTMC) method is used in the kMC simulations. In this method, a list of events is constructed and an event is selected randomly with its respective probability. After the execution of the selected event, the list is updated based on the new lattice configuration. The following values are used for the parameters of the migration rate of Eq. (1), $v_0 = 10^{13}$ s^{-1}, E_s=3.4 eV and E_n=0 eV. Figs. 2 and 3 show that both atomic roughness and slope increase with time and will reach steady-state values at different time scales. Furthermore, both surface roughness and slope increase with total deposition rate w.

To further investigate the open-loop properties of this two species simulation model, simulations are carried out with different deposition rate ratio between the two components. As shown in

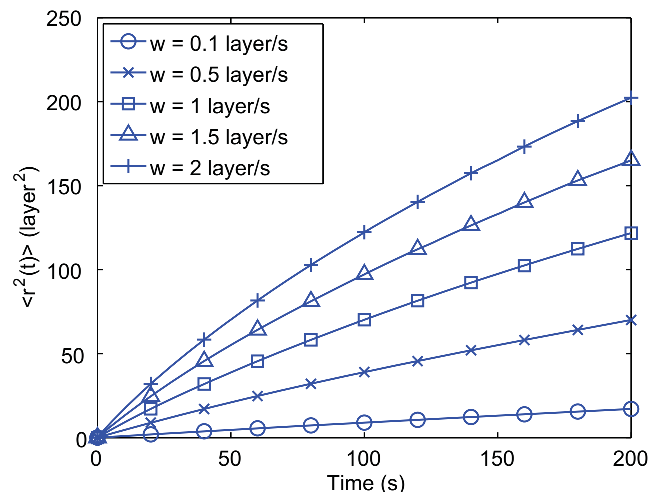

Fig. 2. Evolution of expected atomic surface roughness with respect to time for different deposition rates (unit of w is layer/s) obtained from kMC simulations.

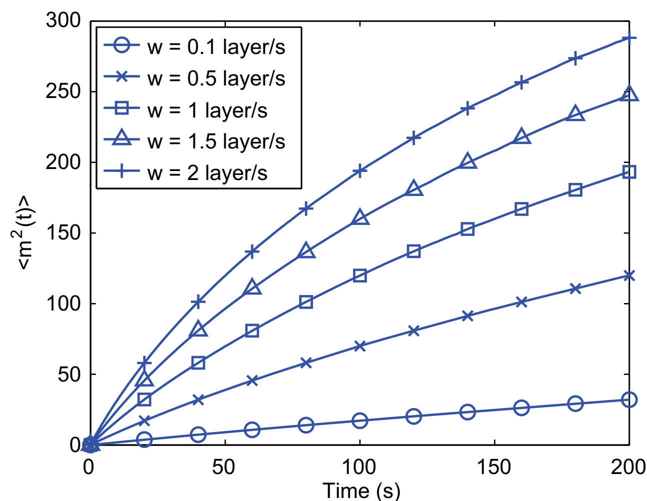

Fig. 3. Evolution of expected atomic surface slope with respect to time for different deposition rates (unit of w is layer/s) obtained from kMC simulations.

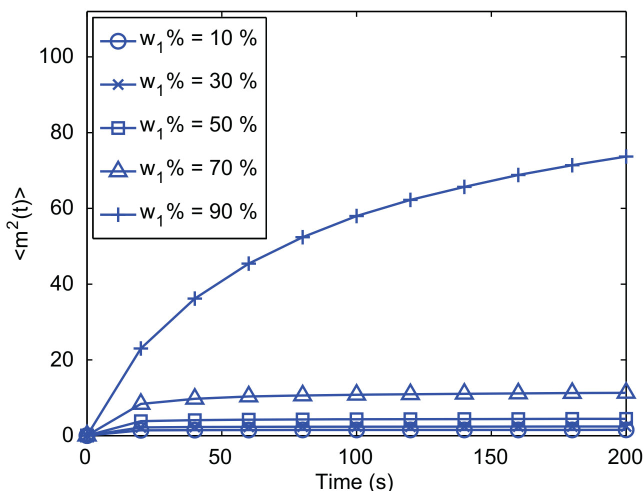

Fig. 5. Evolution of expected atomic surface slope with respect to time for different compositions from two species kMC simulations.

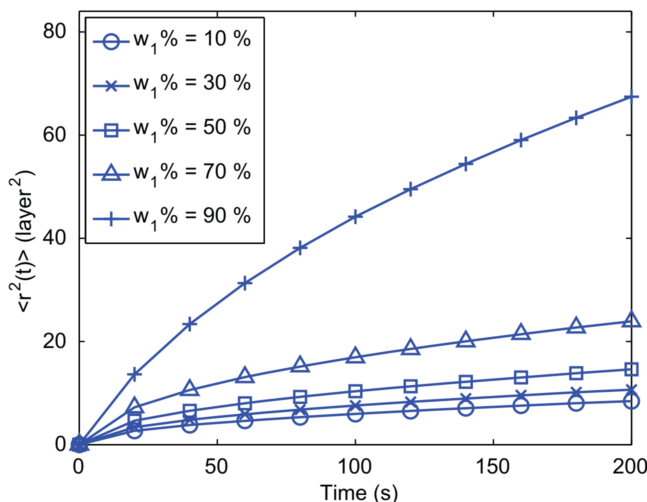

Fig. 4. Evolution of expected atomic surface roughness with respect to time for different compositions from two species kMC simulations.

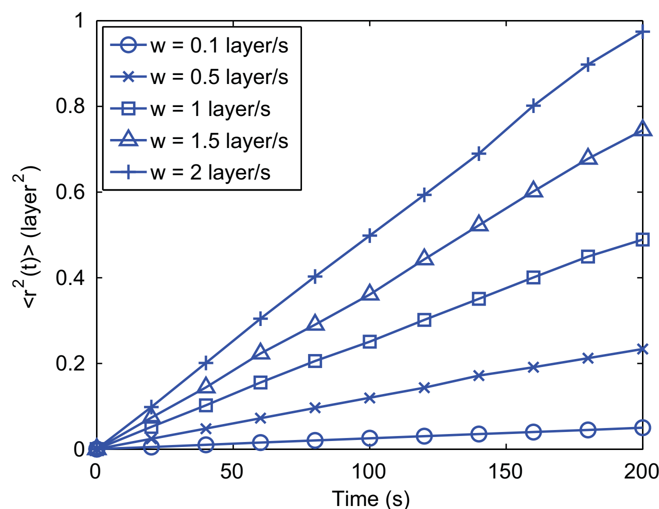

Fig. 6. Evolution of expected aggregate surface roughness with respect to time for different deposition rates (unit of w is layer/s) obtained from kMC simulations.

Figs. 4 and 5, as $w_1\%$ ($w_1\% = w_1/w$) increases, the values of both the roughness and the slope increase since at this temperature ($T = 800$ K), the effect of the migration (which has the ability to smooth the surface compared to the RDSR process) is weak. Thus, as ZnO ($w_1\%$) dominates the deposition process, the surface becomes more rough.

2.2. Aggregate surface morphology and spatial deposition rate profile

One of the most important applications of our work is to simulate and control the deposition process of thin film solar cells in order to improve solar cell efficiency. However, the wavelength of visible light (400–700 nm) is much larger than the diameter of ZnO particles (~ 0.3 nm) and thus, it is necessary to define an aggregate surface morphology at length scales comparable to visible light wavelength (Huang et al., 2011b).

Specifically, the aggregate surface morphology is computed similarly to the atomic surface morphology, but on the basis of the aggregate surface height profile, $h_{\Delta,i}$, which is defined as follows:

$$h_{\Delta,i} = (h_{i\Delta+1} + h_{i\Delta+2} + \cdots + h_{(i+1)\Delta})/\Delta, \quad i = 0, 1, \ldots, L/\Delta - 1 \tag{5}$$

where $h_{\Delta,i}$ denotes the averaged surface height over the length scale of Δ sites, Δ denotes the aggregation size, i.e., the number of lattice sites used to calculate the aggregate surface height, and L/Δ denotes the number of aggregate sites of size Δ included in the spatial domain of the process. For the wavelength of visible light and silicon thin-film solar cells, the corresponding Δ is around 400; this follows from the fact that 0.3 nm $\times$ 400 = 120 nm, which is a length scale comparable to visible light wavelength (Huang et al., 2011b); the same aggregation level is used for the TCO layer in this work. The definition of aggregate surface roughness and slope is given as follows:

$$r_\Delta = \left[\frac{1}{L/\Delta}\sum_{i=1}^{L/\Delta}(h_{\Delta,i} - \bar{h}_\Delta)^2\right]^{1/2},$$

$$m_\Delta = \left[\frac{1}{L/\Delta}\sum_{i=1}^{L/\Delta}\left(\frac{h_{\Delta,i} - h_{\Delta,i+1}}{\Delta}\right)^2\right]^{1/2} \tag{6}$$

The dynamics of aggregate roughness and slope are shown in Figs. 6 and 7. The simulation duration is $t_f = 200$ s and 100 independent simulations were carried out to calculate the expected values of aggregate surface roughness and slope (further increase of the number of independent simulations did not change the expected values). It is clear that at the aggregation length $\Delta = 400$, both $\langle r_\Delta^2(t_f)\rangle$ and $\langle m_\Delta^2(t_f)\rangle$ are much smaller compared to their

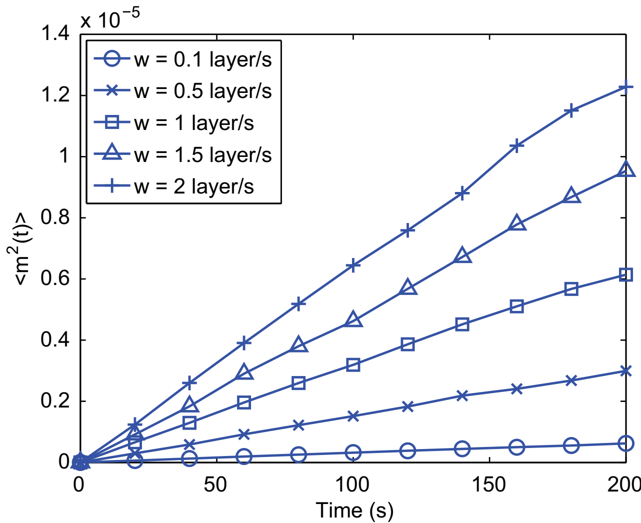

Fig. 7. Evolution of expected aggregate surface slope with respect to time for different deposition rates (unit of w is layer/s) obtained from kMC simulations.

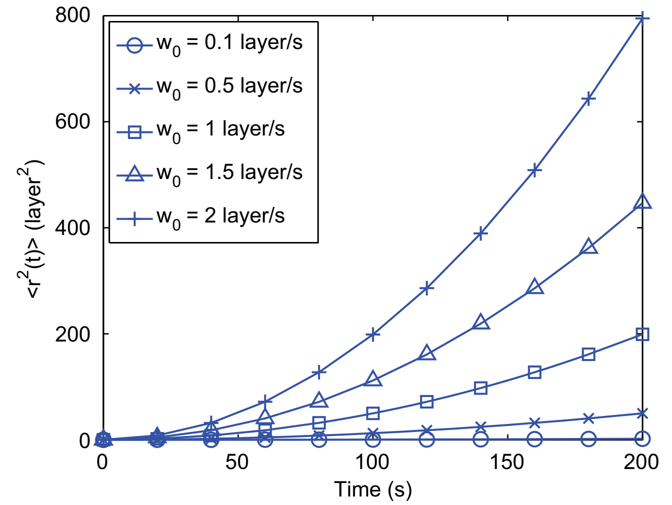

Fig. 8. Evolution of expected aggregate surface roughness with respect to time for different mean deposition rates (unit of w_0 is layer/s) obtained from kMC simulations. Patterned deposition with $k=5$ and $A=0.1w_0$.

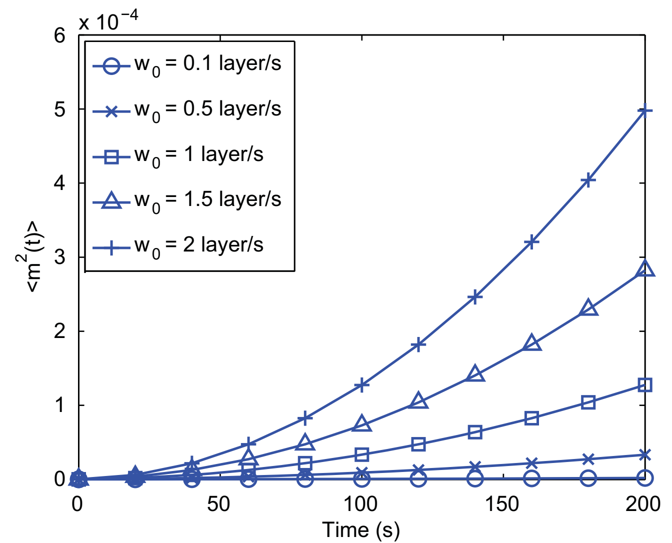

Fig. 9. Evolution of expected aggregate surface slope with respect to time for different mean deposition rates (unit of w_0 is layer/s) obtained from kMC simulations. Patterned deposition with $k=5$ and $A=0.1w_0$.

corresponding value at atomic length scale. It is reported that the desired $\langle r_{\Delta}^2(t_f)\rangle$ for optimum optical performance of TCO thin film ranges from 500 to 10,000 nm^2 (Krč and Zeman, 2003), which is much larger than available aggregate roughness value with practically viable simulation time and deposition rate magnitude. This small aggregate roughness at large characteristic length scales is partly because the operating conditions are spatially uniform throughout the entire deposition process, i.e., the same deposition rate and substrate temperature are applied throughout the spatial domain. Thus, a spatially non-uniform deposition rate profile is necessary for the purpose of optimizing thin film light trapping properties by manipulation of film aggregate surface roughness and slope at length scales comparable to visible light wavelength (Huang et al., 2011b). To this end, we introduce a patterned in space deposition rate profile (see Isabella et al., 2010 for motivation for using such a profile), which is defined as follows:

$$w_1(x)=w_{1,0}+A_1\sin\left(\frac{2k\pi}{L}x\right),\quad A_1\le w_{1,0}$$

$$w_2(x)=w_{2,0}+A_2\sin\left(\frac{2k\pi}{L}x\right),\quad A_2\le w_{2,0}$$

$$w(x)=w_1(x)+w_2(x)$$

$$w_0(x)=w_{1,0}(x)+w_{2,0}(x),\quad A=A_1+A_2 \tag{7}$$

where x is a position along the lattice, $w_{1,0}$ and $w_{2,0}$ are the mean deposition rates, A_1 and A_2 are the magnitude of the patterned deposition profile, k is the number of sine waves along the entire lattice, and L is the lattice size. It is assumed that $w_1:w_2=w_{1,0}:w_{2,0}=A_1:A_2=24:1$.

The dynamics of aggregate surface morphology with patterned deposition rate profile is studied by carrying out a series of simulations at different mean deposition rates w_0 with $L=40{,}000$, $\Delta=400$, $T=800$ K, $k=5$ and $A=0.1w_0$. The evolution profiles for aggregate roughness and slope are shown in Figs. 8 and 9. The introduction of patterned deposition rate profiles significantly changes the dynamic profiles of aggregate surface morphology. However, some properties obtained under uniform deposition rate evolution profiles remain valid, for example, the expected values of aggregate surface roughness and slope still increase with mean deposition rate w_0. Furthermore, simulations are carried out at $w_0=2$ layer/s with different magnitude, A, values to investigate the influence of the strength of patterned deposition on the evolution profiles of aggregate surface morphology. As shown in Figs. 10 and 11, the magnitude, A, has substantial influence on the dynamics of aggregate surface morphology. Both aggregate roughness and aggregate slope can be increased substantially by manipulating A compared to the aggregate surface morphology achieved with a uniform deposition rate profile. Thus, the introduction of a patterned deposition rate profile expands the range of surface morphology values that can be obtained and makes surface morphology control at length scales comparable to visible light wavelength possible.

3. Closed-form modeling and parameter estimation

3.1. Edward–Wilkinson type equation of aggregate surface height

Given the complexity of the two species deposition process and the need to control surface roughness and slope at spatial scales comparable to the wavelength of visible light, the direct

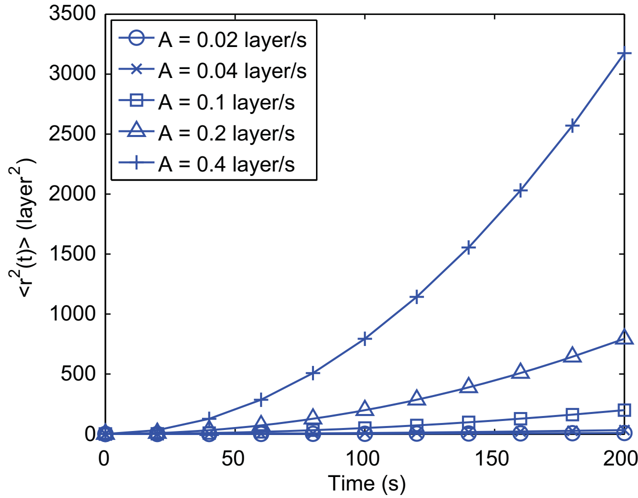

Fig. 10. Evolution of expected aggregate surface roughness with respect to time for different patterned deposition rate magnitudes obtained from kMC simulations. Patterned deposition with $k=5$ and $w_0=2$ layer/s.

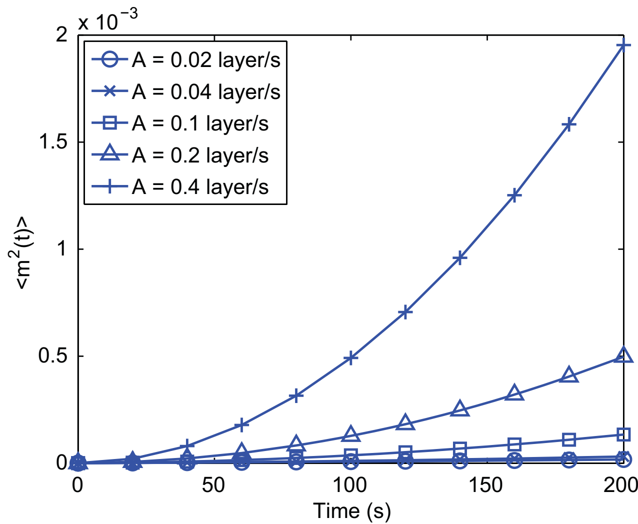

Fig. 11. Evolution of expected aggregate surface slope with respect to time for different patterned deposition rate magnitudes obtained from kMC simulations. Patterned deposition with $k=5$ and $w_0=2$ layer/s.

computation of a closed-form model, describing the surface height evolution and is suitable for controller design, from the microscopic deposition mechanisms is a very difficult (if not impossible) task. Therefore, a hybrid modeling approach should be used in which a basic closed-form modeling structure is used and the model parameters are computed such that the predictions of key variables from the closed-form model are close to the one of the kinetic Monte–Carlo model for a broad set of operating conditions. To this end, we use an Edward–Wilkinson (EW) type equation, which is a second-order stochastic PDE, to describe the aggregate surface height evolution and compute its parameters from kMC data. The choice of the EW-equation is motivated by the fact that it has been used in many deposition processes that involve a thermal balance between adsorption and relaxation/migration (Buzea and Robbie, 2005). Specifically, a one-dimensional EW-type equation is used to describe the evolution of aggregate surface height profile

$$\frac{\partial h_\Delta}{\partial t} = w(x,t) + c_2 \frac{\partial^2 h_\Delta}{\partial x^2} + \xi(x,t) \tag{8}$$

subject to the following periodic boundary conditions

$$h_\Delta(0,t) = h_\Delta(L,t) \tag{9}$$

$$\frac{\partial h_\Delta}{\partial x}(0,t) = \frac{\partial h_\Delta}{\partial x}(L,t) \tag{10}$$

and the initial condition

$$h_\Delta(x,0) = h_\Delta^0(x) \tag{11}$$

where $x \in [0,L]$ is the spatial coordinate, t is the time, $h_\Delta(x,t)$ is the aggregate surface height and $\xi(x,t)$ is a Gaussian white noise with zero mean and the following covariance:

$$\langle \xi(x,t)\xi(x',t') \rangle = \sigma^2 \delta(x-x')\delta(t-t') \tag{12}$$

where $\delta(\cdot)$ denotes the Dirac delta function. In Eq. (8), the parameters c_2 and σ^2, corresponding to diffusion effects and stochastic noise respectively, depend on the deposition rate $w(x,t)$. In the case of a patterned deposition rate profile (control actuation), the term $w(x,t)$ is of the form

$$w(x,t) = w_0(t) + A(t)\sin\left(\frac{2k\pi}{L}x\right) \tag{13}$$

where $w_0(t)$ is the total mean deposition rate and $A(t)$ is the total magnitude of patterned deposition rate. In the context of two species simulations, $w(x,t)$, $w_0(t)$ and $A(t)$ can be seen as the sum of corresponding values from each component (i.e., $w(x,t) = w_1(x,t) + w_2(x,t)$, $w_0(t) = w_{1,0}(t) + w_{2,0}(t)$, $A(t) = A_1(t) + A_2(t)$) and k is the number of sine waves between 0 and L.

To analyze the dynamics and obtain a solution of the EW equation suitable for real-time controller calculations, we first consider the eigenvalue problem of the linear operator of Eq. (8) subject to the periodic boundary conditions of Eqs. (9) and (10)

$$\mathcal{A}\overline{\phi}_n(x) = c_2 \frac{d^2\overline{\phi}_n(x)}{dx^2} = \lambda_n \overline{\phi}_n(x) \tag{14}$$

$$\nabla^j \overline{\phi}_n(0) = \nabla^j \overline{\phi}_n(L), \quad j = 0, 1 \tag{15}$$

where λ_n denotes an eigenvalue, $\overline{\phi}_n$ denotes an eigenfunction, and ∇^j, $j=0, 1$, denotes the gradient of a given function. The solution of the eigenvalue problem of Eqs. (14) and (15) is as follows:

$$\lambda_n = -\frac{4c_2\pi^2 n^2}{L^2} \tag{16}$$

$$\phi_{1,n}(x) = \phi_n = \sqrt{\frac{2}{L}}\sin\left(\frac{2n\pi}{L}x\right) \tag{17}$$

$$\phi_{2,n}(x) = \psi_n = \begin{cases} \sqrt{\dfrac{1}{L}}, & n = 0 \\ \sqrt{\dfrac{2}{L}}\cos\left(\dfrac{2n\pi}{L}x\right), & n \neq 0 \end{cases} \tag{18}$$

The solution of the EW equation of Eq. (8) can be expanded in an infinite series in terms of the eigenfunctions of the spatial differential operator of Eq. (14) as follows:

$$h_\Delta(x,t) = \sum_{n=0}^{L/(2\Delta)} (\phi_{1,n}(x)z_{1,n}(t) + \phi_{2,n}(x)z_{2,n}(t)), \tag{19}$$

where $z_{1,n}(t)$, $z_{2,n}(t)$ are time-varying coefficients.

Substituting the above expansion for the solution, $h_\Delta(x,t)$, into Eq. (8) and taking the inner product with the adjoint eigenfunctions, the following system of infinite stochastic linear ordinary differential equations (ODEs) for the temporal evolution of the time-varying coefficients in Eq. (19) is obtained

$$\frac{dz_{2,0}(t)}{dt} = w_{2,0} + \xi_{2,0}(t), \tag{20}$$

$$\frac{dz_{p,n}(t)}{dt} = w_{p,n} + \lambda_n z_{p,n} + \xi_{p,n}(t), \quad p = 1,2, \quad n = 1,\ldots,\frac{L}{2\Delta}, \tag{21}$$

where $\xi_{p,n}(t) = \int_0^L \xi(x,t)\phi_{p,n}(x)\,dx$ is the projection of the noise $\xi(x,t)$ on the ODE for $z_{p,n}$. The noise term, $\xi_{p,n}$, has zero mean and covariance

$$\langle \xi_{p,n}(t)\xi_{p,n}(t')\rangle = \sigma^2\delta(t-t'). \tag{22}$$

Similarly, $w_{p,n}$ is the projection of w on the ODE for $z_{p,n}(t)$, $w_{p,n} = \int_0^L \phi_{p,n}(x)w(x)\,dx$

- If $p=1$,

$$w_{1,n} = \begin{cases} 0, & n \neq k \\ A\sqrt{\dfrac{L}{2}}, & n = k \end{cases} \tag{23}$$

- If $p=2$,

$$w_{2,n} = \begin{cases} 0, & n \neq 0 \\ A\sqrt{L}, & n = 0 \end{cases} \tag{24}$$

The temporal evolution of the variance of mode $z_{p,n}$ can be obtained from the solution of the linear ODEs of Eqs. (20) and (21) as follows:

$$\langle z_{2,0}(t)\rangle = w_{2,0}(t-t_0) \tag{25}$$

$$\mathrm{var}(z_{2,0}(t)) = \sigma^2(t-t_0) \tag{26}$$

$$\langle z(t)\rangle = e^{\lambda(t-t_0)}\langle z(t_0)\rangle + \frac{w_p}{\lambda}(e^{\lambda(t-t_0)}-1) \tag{27}$$

$$\mathrm{var}(z(t)) = e^{2\lambda(t-t_0)}\,\mathrm{var}(z(t_0)) + \sigma^2\frac{e^{2\lambda(t-t_0)}-1}{2\lambda} \tag{28}$$

where $z(t) = z_{p,n}(t)$, $\lambda = \lambda_n$ and $w_p = w_{p,n}$ for $n \neq 0$.

Finally, it is necessary to point out that, when aggregate (discrete) surface height profile is used, the highest number of modes that can be accurately estimated from $h_\Delta(x,t)$ is limited by the spatial sampling points, $n \leq L/2\Delta$; the reader may refer to Zhang et al. (2012) for a detailed discussion of the issue.

3.2. Aggregate surface root-mean-square roughness

Aggregate surface roughness of the thin film is defined as the standard deviation of the aggregate surface height profile from its average height

$$r_\Delta(t) = \sqrt{\frac{1}{L}\int_0^L [h_\Delta(x,t) - \overline{h}_\Delta(t)]^2\,dx} \tag{29}$$

where $\overline{h}_\Delta(t) = (1/L)\int_0^L h_\Delta(x,t)\,dx$ is the average aggregate surface height. According to Eq. (19), we have

$$\overline{h}_\Delta(t) = \frac{1}{L}\int_0^L \phi_{2,0}z_{2,0}\,dx = \sqrt{\frac{1}{L}}z_{2,0} \tag{30}$$

Using that

$$h_\Delta(x,t) - \overline{h}_\Delta(t) = \sum_{n=1}^{L/(2\Delta)}\sum_{p=1}^{2}\phi_{p,n}(x)z_{p,n}(t) \tag{31}$$

the expected aggregate surface roughness, $\langle r_\Delta^2(t)\rangle$, of Eq. (29) can be re-written as

$$\begin{aligned}\langle r_\Delta^2(t)\rangle &= \left\langle \frac{1}{L}\int_0^L \left[\sum_{p=1}^{2}\sum_{n=1}^{L/(2\Delta)} z_{p,n}(t)\phi_{p,n}(x)\right]^2 dx\right\rangle \\ &= \left\langle \frac{1}{L}\int_0^L \sum_{n=1}^{L/(2\Delta)} (\phi_{1,n}^2(x)z_{1,n}^2(t) + \phi_{2,n}^2(x)z_{2,n}^2(t))\,dx\right\rangle \\ &= \frac{1}{L}\sum_{n=1}^{L/(2\Delta)}(\langle z_{1,n}^2\rangle + \langle z_{2,n}^2\rangle)\end{aligned} \tag{32}$$

where

$$\langle z_{p,n}^2\rangle = \mathrm{var}(z_{p,n}) + \langle z_{p,n}\rangle^2 \tag{33}$$

The expression of Eqs. (32) and (33) will be used in the MPC formulation; see Eq. (42) below.

3.3. Aggregate surface root-mean-square slope

The aggregate RMS slope is defined as the root-mean-square of the aggregate surface slope in the x-direction as follows:

$$m_\Delta(t) = \sqrt{\frac{1}{L}\int_0^L \left(\frac{\partial h_\Delta}{\partial x}\right)^2 dx} = \sqrt{\frac{1}{L}\sum_{i=0}^{L/\Delta}\left(\frac{h_\Delta(i+1,t) - h_\Delta(i,t)}{\Delta}\right)^2 \Delta} \tag{34}$$

Using the expansion of Eq. (19), Eq. (34) can be written as:

$$\begin{aligned}\langle m_\Delta^2(t)\rangle &= \left\langle \frac{1}{L}\sum_{i=0}^{L/\Delta}\left(\frac{h_\Delta(i+1,t) - h_\Delta(i,t)}{\Delta}\right)^2 \Delta\right\rangle \\ &= \left\langle \frac{1}{L\Delta}\sum_{i=0}^{L/\Delta}\left\{\sum_{p=1}^{2}\sum_{n=0}^{L/(2\Delta)} z_{p,n}[\phi_{p,n}(i+1) - \phi_{p,n}(i)]\right\}^2\right\rangle \\ &= \left\langle \frac{1}{L\Delta}\sum_{i=0}^{L/\Delta}\sum_{p_1=1}^{2}\sum_{n_1=0}^{L/(2\Delta)}\sum_{p_2=1}^{2}\sum_{n_2=0}^{L/(2\Delta)} z_{p_1,n_1}z_{p_2,n_2}\,d\phi_{p_1,n_1}(i)\,d\phi_{p_2,n_2}(i)\right\rangle \\ &= \frac{1}{L\Delta}\sum_{p_1=1}^{2}\sum_{n_1=0}^{L/(2\Delta)}\sum_{p_2=1}^{2}\sum_{n_2=0}^{L/(2\Delta)}\langle z_{p_1,n_1}z_{p_2,n_2}\rangle\left(\sum_{i=0}^{L/\Delta} d\phi_{p_1,n_1}(i)\,d\phi_{p_2,n_2}(i)\right)\end{aligned} \tag{35}$$

where

$$\begin{aligned}&\sum_{i=0}^{L/\Delta} d\phi_{p_1,n_1}(i)\,d\phi_{p_2,n_2}(i) \\ &\quad= \sum_{i=0}^{L/\Delta}(\phi_{p_1,n_1}(i+1) - \phi_{p_1,n_1}(i))(\phi_{p_2,n_2}(i+1) - \phi_{p_2,n_2}(i)) \\ &\quad= \frac{2}{L}\left(\sum_{i=0}^{L/\Delta}\left(\sin\left(\frac{2n_1\pi}{L/\Delta}(i+1)\right) - \sin\left(\frac{2n_1\pi}{L/\Delta}i\right)\right)\right. \\ &\qquad\left.\times\left(\sin\left(\frac{2n_2\pi}{L/\Delta}(i+1)\right) - \sin\left(\frac{2n_2\pi}{L/\Delta}i\right)\right)\right) \\ &\quad= \frac{8}{L}\sin\left(\frac{n_1\pi}{L/\Delta}\right)\sin\left(\frac{n_2\pi}{L/\Delta}\right)\sum_{i=0}^{L/\Delta}\left(\cos\left(\frac{n_1\pi}{L/\Delta}(2i+1)\right)\right. \\ &\qquad\left.\times\cos\left(\frac{n_2\pi}{L/\Delta}(2i+1)\right)\right)\end{aligned} \tag{36}$$

or more compactly

$$\begin{aligned}\langle m_\Delta^2(t)\rangle &= \frac{1}{L\Delta}\sum_{p_1=1}^{2}\sum_{n_1=0}^{L/(2\Delta)}\sum_{p_2=1}^{2}\sum_{n_2=0}^{L/(2\Delta)}\langle z_{p_1,n_1}z_{p_2,n_2}\rangle \\ &\qquad\times\left(\sum_{i=0}^{L/\Delta} d\phi_{p_1,n_1}(i)\,d\phi_{p_2,n_2}(i)\right) \\ &= \frac{1}{L\Delta}\sum_{p=1}^{2}\sum_{n=0}^{L/(2\Delta)}\langle z_{p,n}\rangle^2\left(\frac{8}{L}\sin^2\left(\frac{n\pi}{L/\Delta}\right)\sum_{i=0}^{L/\Delta}\left(\cos^2\left(\frac{n\pi}{L/\Delta}(2i+1)\right)\right)\right) \\ &= \sum_{p=1}^{2}\sum_{n=0}^{L/(2\Delta)} K_{p,n}\langle z_{p,n}^2\rangle\end{aligned} \tag{37}$$

where

$$K_{p,n} = \frac{8}{L^2\Delta}\sin^2\left(\frac{\pi n}{L/\Delta}\right)\sum_{i=0}^{L/(2\Delta)}\left(\cos^2\left(\frac{n\pi}{L/\Delta}(2i+1)\right)\right) = \begin{cases} \frac{8}{L\Delta^2}\sin^2\left(\frac{\pi n}{L/\Delta}\right) & n=0 \\ \frac{4}{L\Delta^2}\sin^2\left(\frac{\pi n}{L/\Delta}\right) & n\neq 0 \end{cases} \quad (38)$$

Finally, using that

$$\sum_{i=0}^{L/(2\Delta)}\left(\cos^2\left(\frac{n\pi}{L/\Delta}(2i+1)\right)\right) = \sum_{i=0}^{L/(2\Delta)}\left(\frac{\cos(2n\pi(2i+1)/(L/\Delta))+1}{2}\right) = \begin{cases} \frac{L}{\Delta} & \text{if } n=0 \\ \frac{L}{2\Delta} & \text{if } n\neq 0 \end{cases} \quad (39)$$

$\langle m_\Delta^2(t)\rangle$ can be expressed as

$$\langle m^2(t)\rangle = \sum_{m=1}^{L/(2\Delta)}(K_{1,m}\langle z_{1,m}^2\rangle + K_{2,m}\langle z_{2,m}^2\rangle) \quad (40)$$

The expression of Eq. (40) will be used in the MPC formulation; see Eq. (42) below.

3.4. Parameter estimation

Referring to the EW equation of Eq. (8), there are two model parameters, c_2 and σ^2, that must be determined as functions of the total mean deposition rate w_0 and of the total patterned deposition rate magnitude A. These parameters affect the dynamics of aggregate surface roughness and slope and can be estimated by fitting the predicted evolution profiles for aggregate surface roughness and slope from the EW equation to profiles of aggregate surface roughness and slope from kMC simulations. Least-square methods are used to estimate the model parameters so that the EW-model predictions are close in a least-square sense to the kMC simulation data. Comparison of the predictions of both models are shown in Fig. 12. Based on c_2 and σ^2 values obtained from these fitting results, different functions are chosen to estimate c_2 and σ^2 values at different w with the least-square method. Specifically, a linear function with respect to log(w) is chosen to estimate log(c_2) and a linear function with respect to w is chosen to estimate σ^2, and the expressions are given as follows:

$$c_2(w) = w_{c_2}^{a} \cdot e_{c_2}^{b}$$

$$\sigma^2 = a_{\sigma^2}w + b_{\sigma^2} \quad (41)$$

where a_{c_2}, b_{c_2}, a_{σ^2} and b_{σ^2} are time-invariant fitting model parameters. The fitting results are shown in Figs. 13 and 14. To verify the fitting function, two more groups of simulations are carried out with larger deposition rates (w=5 and 10 layer/s) and fitted to EW equation, and the obtained values for c_2 and σ^2 are used to extend the fitting curve to show the validity of the chosen fitting functions. It is necessary to clarify that these fitting results are based on kMC simulations with uniform deposition rate profiles (A=0). For simulations with patterned deposition rate profiles ($A \neq 0$), it is assumed that c_2 and σ^2 models obtained from uniform deposition rate

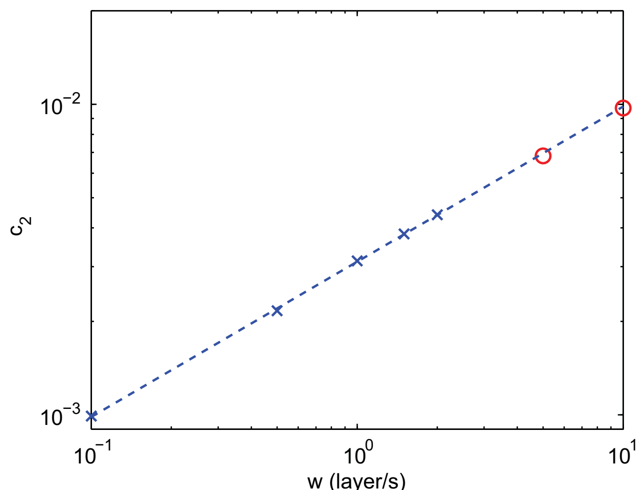

Fig. 13. c_2 values for different spatially uniform deposition rates w. The solid line is the result of a linear fitting function and it is the log(c_2) versus log(w) relationship used by the predictive controller. The first 5 blue cross-markers are used to generate the fitting function, and the last 2 red circle markers are used to test the validity of the fitting function. (For interpretation of the references to color in this figure legend, the reader is referred to the web version of this article.)

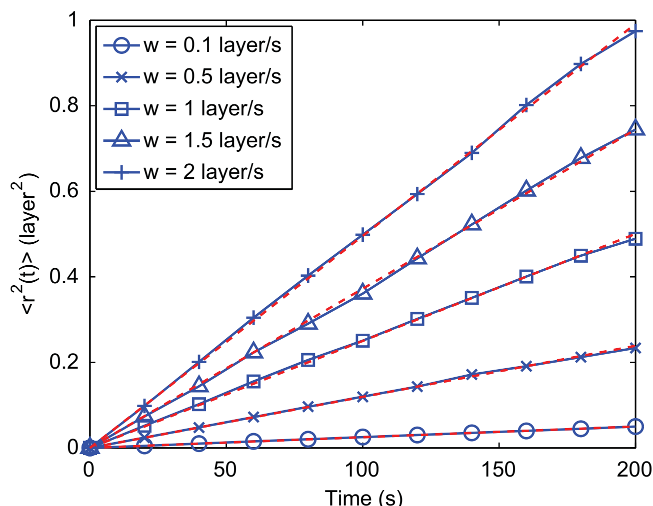

Fig. 12. Evolution of expected aggregate surface roughness with respect to time for different spatially uniform deposition rates obtained from kMC simulations (solid lines with symbols). The analytical solutions for the aggregate surface roughness obtained from the corresponding EW equations with the fitted values for c_2 and σ^2 are also shown (dashed lines).

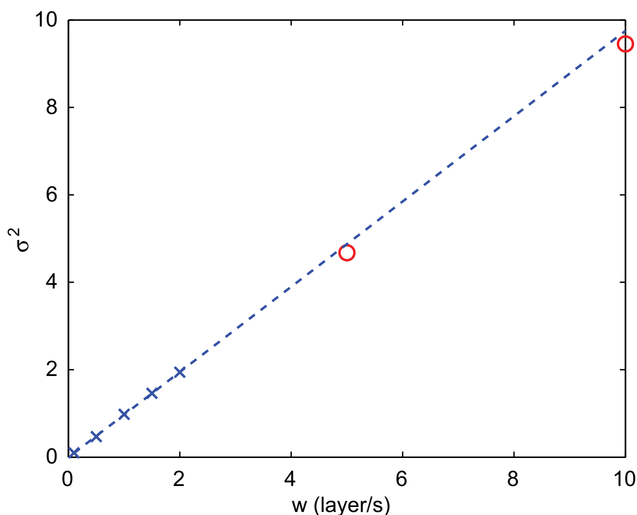

Fig. 14. σ^2 values for different spatially uniform deposition rates w. The solid line is the result of a linear fitting function. The first 5 blue cross-markers are used to generate the fitting function, and the last 2 red circle markers are used to test the validity of the fitting function. (For interpretation of the references to color in this figure legend, the reader is referred to the web version of this article.)

simulations ($A=0$) can be used to estimate c_2 and σ^2 values. To verify this assumption, the solutions of EW equations for aggregate surface evolution with patterned deposition rate profile are obtained based on c_2 and σ^2 models from open-loop kMC data with uniform deposition rate, and these dynamic evolution profiles are compared with open-loop kMC dynamic evolution profiles with patterned deposition rate profiles. As shown in Figs. 15 and 16, c_2 and σ^2 models from open-loop kMC data with uniform deposition rate can be used in the EW equation to predict aggregate surface roughness and slope of the kMC model with patterned deposition rate. We note that the approach presented for the computation of the parameters of the closed-form PDE model of Eq. (8) is not limited to the specific PDE system and can be used in the context of other dissipative PDE systems that model the evolution of surface height of deposition processes. Finally, referring to the dependence of surface roughness and slope on lattice size, we note that both atomic and aggregate surface roughness and slope increase with increasing lattice size (this issue has been extensively studied in another work Huang et al., 2011a); however, the proposed approach to closed-form modeling and MPC design is scalable and can be used in the context of different lattice size kMC models as long as the parameters of the stochastic PDE model of Eq. (8) and their dependence on deposition rate are computed on the basis of data obtained from the lattice size considered.

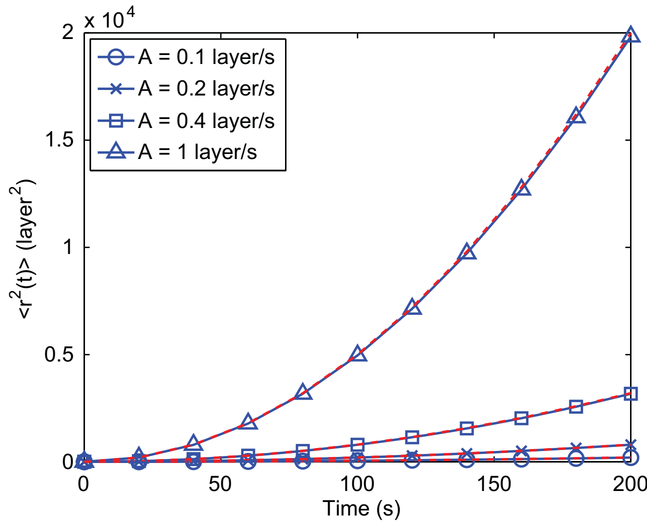

Fig. 15. Evolution of expected aggregate surface roughness for different patterned deposition magnitudes from the kMC model (solid lines with symbols) and expected aggregate roughness solutions from the corresponding EW equations (dashed lines). The c_2 and σ^2 values of the EW equations were estimated from open-loop aggregate surface roughness kMC model data with spatially uniform deposition rates.

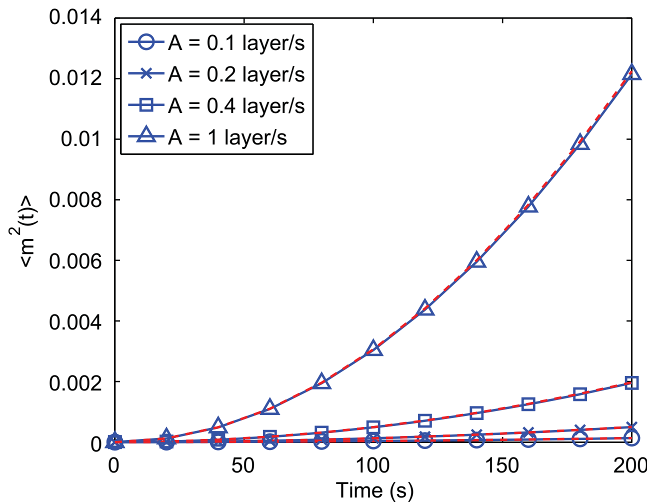

Fig. 16. Evolution of expected aggregate surface slope for different patterned deposition magnitudes from the kMC model (solid lines with symbols) and expected aggregate slope solutions from the corresponding EW equations (dashed lines). The c_2 and σ^2 values of the EW equations were estimated from open-loop aggregate surface roughness kMC model data with spatially uniform deposition rates.

4. Model predictive control

In this section, we design a model predictive controller based on the dynamic models of aggregate surface roughness and slope to simultaneously control the expected values of aggregate surface roughness and slope square to desired levels. The dynamics of aggregate surface roughness and slope of the TCO thin film are described by the EW equation of aggregate surface height of Eq. (8) with the computed parameters of Section 3.4. State feedback control is considered in this work, i.e., $h_\Delta(x,t)$ is assumed to be available for feedback. In practice, real-time surface height measurements can be obtained via atomic force microscopy (AFM) systems.

4.1. MPC formulation for regulation of aggregate roughness and slope

We consider the problem of regulation of aggregate surface roughness and slope to desired levels within a model predictive control framework. Due to the stochastic nature of the variables, the expected values of aggregate surface roughness and slope, $\langle r_\Delta^2(t)\rangle$ and $\langle m_\Delta^2(t)\rangle$, are chosen as the control objectives. The total mean deposition rate, w_0 ($w_0 = w_{1,0}+w_{2,0}$), and magnitude of patterned deposition rate, A ($A=A_1+A_2$), are chosen as the manipulated inputs; the substrate temperature is fixed at $T=800$ K during all closed-loop simulations. To account for a number of practical considerations, several constraints are added to the control problem. In particular, since $w(x)\geq 0$, the constraint $0\leq A_1\leq w_{1,0}$ and $0\leq A_2\leq w_{2,0}$ are imposed to ensure $w(x,t)>0$, $\forall(x,t)$. To ensure the validity of the closed-form process model, there is a constraint on the range of variation of the mean deposition rate. Another constraint is imposed on the rate of change of the mean deposition rate to account for actuator limitations. The control action at time t is obtained by solving a finite-horizon optimal control problem. The cost function in the optimal control problem includes penalty on the deviation of $\langle r_\Delta^2\rangle$ and $\langle m_\Delta^2\rangle$ from their respective set-point values. Different weighting factors are assigned to the aggregate surface roughness and slope. Aggregate surface roughness and slope have very different magnitudes, therefore, relative deviations are used in the formulation of the cost function to make the magnitude of the two terms comparable in the cost function. The optimization problem is subject to the dynamics of the aggregate surface height of Eq. (8). The optimal w_0 and A values are calculated at each sampling time by solving a finite-dimensional optimization problem in a receding horizon fashion. Specifically, the MPC problem at time t is formulated as follows:

$$\min_{w_0,A} f(w_0,A) = q_{r^2}\left[\frac{r_{set}^2-\langle r_\Delta^2(t_f)\rangle}{r_{set}^2}\right]^2 + q_{m^2}\left[\frac{m_{set}^2-\langle m_\Delta^2(t_f)\rangle}{m_{set}^2}\right]^2 \quad (42)$$

where

$$\langle r_\Delta^2(t_f)\rangle = \frac{1}{L}\sum_{n=1}^{L/(2\Delta)}\sum_{p=1}^{2}\langle z_{p,n}^2(t_f)\rangle,$$

$$\langle m_\Delta^2(t_f)\rangle = \sum_{n=1}^{L/(2\Delta)}\sum_{p=1}^{2}(K_{p,n}\langle z_{p,n}^2(t_f)\rangle) \quad (43)$$

$$\langle z_{p,n}^2(t_f)\rangle = \text{var}(z_{p,n}(t_f)) + \langle z_{p,n}(t_f)\rangle^2 \quad (44)$$

$$\langle z_{p,n}(t_f)\rangle = e^{\lambda_n(t_f-t)}\langle z_{p,n}(t)\rangle + \frac{w_p}{\lambda_n}(e^{\lambda_n(t_f-t)}-1) \quad (45)$$

$$\text{var}(z_{p,n}(t_f)) = e^{2\lambda_n(t_f-t)}\,\text{var}(z_{p,n}(t)) + \sigma^2(w)\frac{e^{2\lambda_n(t_f-t)}-1}{2\lambda_n} \quad (46)$$

$$\lambda_n = -\frac{4c_2(w)\pi^2}{L^2}n^2 \quad (47)$$

and

$$c_2(w_0) = w_0^{a_{c_2}} \cdot e_{c_2}^{b} \quad (48)$$

$$\sigma^2(w_0) = a_{\sigma^2}w_0 + b_{\sigma^2} \quad (49)$$

subject to:

$$w_{min} \le w_0 \le w_{max}, \quad |w_0(t) - w_0(t-dt)| \le \delta w_{max} \quad (50)$$

$$w_1 = w_{1,0} + A_1 \sin\left(\frac{k\pi x}{L}\right), \quad 0 \le A_1 \le w_{1,0} \quad (51)$$

$$w_2 = w_{2,0} + A_2 \sin\left(\frac{k\pi x}{L}\right), \quad 0 \le A_2 \le w_{2,0} \quad (52)$$

where t is the current time, dt is the sampling time, q_{r^2} and q_{m^2} are the weighting penalty factors for the deviations of $\langle r_\Delta^2\rangle$ and $\langle m_\Delta^2\rangle$ from their respective set-points at the ith prediction step, w_{min} and w_{max} are the lower and upper bounds on the mean deposition rate, respectively, and δw_{max} is the limit on the rate of change of the mean deposition rate. Given the batch nature of the deposition process, the MPC of Eq. (42) includes penalty on the discrepancy of the expected surface roughness and slope at the end of the deposition from the set-points values of surface roughness and slope that lead to desired film reflectance levels. The prediction horizon used in the MPC is the time duration from the current time t to the final time t_f but only one optimal manipulated input value is computed and it is implemented from t to $t+dt$.

The optimal control actions are obtained from the solution of the multivariable optimization problem of Eq. (42) and are applied to the deposition process model over dt (i.e., either the EW equation model or the kMC model) during the time interval $(t, t+dt)$. At time $t+dt$, a new measurement of aggregate surface roughness and slope is received by the controller and the MPC problem of Eq. (42) is solved for the next set of control actions. An interior point method optimizer, IPOPT (Wächter and Biegler, 2006), is used to solve the optimization problem in the MPC formulation and compute a locally optimal solution. With respect to the stability of the closed-loop system, we note the following: the deposition process considered including atom adsorption and atom migration is an inherently stable process; this is evident by the negative values of all the eigenvalues of the spatial differential operator of the Edwards–Wilkinson type equation (Eq. (8)) used to model the evolution of surface height for all values of the deposition rare. Given this stability property of the open-loop process and the specific MPC design, the stability of the closed-loop system is ensured.

5. Simulation results

In this section, the model predictive controller of Eq. (42) is applied to both the one-dimensional EW equation type model of Eq. (8) and the one-dimensional kMC model of the thin film growth process. The mean deposition rate ranges from 0.1 to 2 layer/s, the substrate temperature is fixed at 800 K, the lattice size of the kMC model is fixed at 40,000 sites, the aggregation size is fixed at 400 to make the results relevant to thin film solar cell applications and five sine waves are used in the patterned deposition rate profile. The sampling time is 10 s; this sampling time is enough for the MPC to carry out the calculations needed to compute the control action. In addition to the deposition rate, the temperature may be used as a manipulated input but it should vary in space to induce substantial aggregate surface roughness and slope values at spatial scales corresponding to the visible light wavelength. Each closed-loop simulation lasts for 200 s. Expected values are calculated from 10 independent closed-loop system simulation runs. In all the simulations, the aggregate surface roughness and slope set-points remain the same, specifically, $r_{set}^2 = 1000$ and $m_{set}^2 = 0.005$.

5.1. MPC application to EW equation model

In this subsection, the EW equation model is utilized in the closed-loop control problem as the plant model. First, the problem of regulating aggregate surface roughness is considered. In this problem, the cost function includes only penalty on the deviation of the expected aggregate surface roughness square from its set-point, *i.e.*, $q_{r^2} = 1$ and $q_{m^2} = 0$. Fig. 17 shows the evolution profile of $\langle r_\Delta^2(t)\rangle$ under the model predictive controller of Eq. (42). It is clear that the controller drives the expected aggregate surface roughness to its set-point at the end of the simulation. Fig. 18 shows the input profiles of w_0 and A for these simulations. It is necessary to point out that during the first 40 s of the simulation time, the optimal solutions of w_0 are constrained by the rate of change constraint and the optimal solutions of A are bounded by the values of w_0.

Next, the aggregate surface slope is regulated. The cost function includes only penalty on the deviation of the expected value of aggregate surface slope square from its set-point ($q_{m^2} = 1$, $q_{r^2} = 0$). Fig. 19 shows the evolution profile of the expected aggregate slope square. The aggregate slope reaches its set-point at $t = 200$ s. Fig. 20 displays the input profile in this scenario.

The next step is the simultaneous regulation of aggregate surface roughness and slope. The weighting factor of aggregate slope square, q_{r^2}, is kept at 1, while the weighting factor of aggregate roughness square, q_{m^2}, increases from 10^{-2} to 10^4. Fig. 21 shows the values of expected aggregate surface roughness and slope at the end of closed-loop simulations ($t_f = 200$ s) as a function of q_{m^2}/q_{r^2}. It can be seen that as the weighting on aggregate roughness increases, the expected value of aggregate roughness approaches its set-point at the cost of larger deviation of the aggregate slope from its set-point.

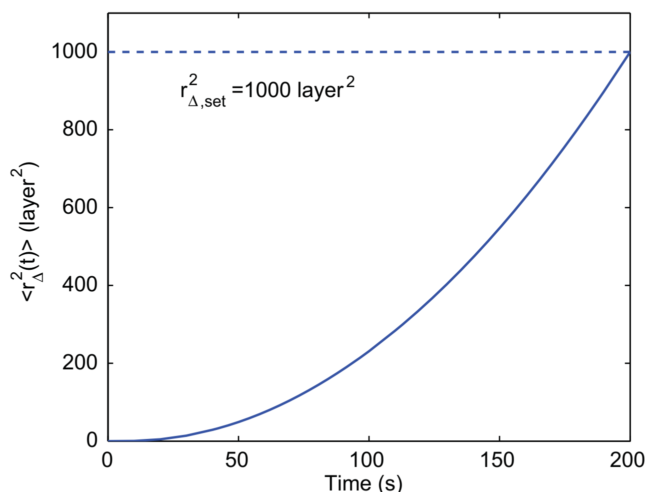

Fig. 17. Profile of expected aggregate surface roughness square with EW equation as the plant model. $q_{r^2} = 1$, $q_{m^2} = 0$ and $r_{set}^2 = 1000$.

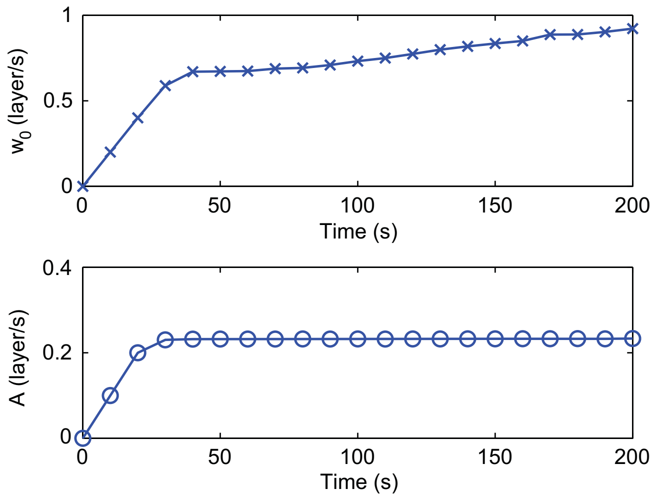

Fig. 18. Input profiles for aggregate roughness-only control problem with EW equation as the plant model. $q_{r^2}=1$, $q_{m^2}=0$ and $r^2_{set}=1000$.

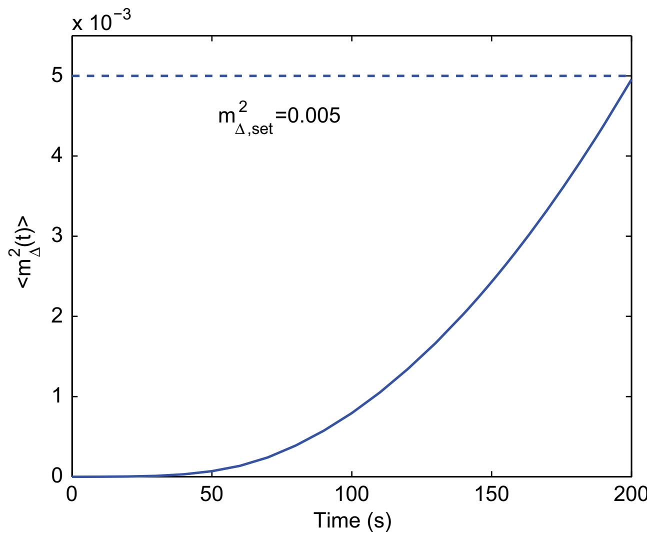

Fig. 19. Profile of expected aggregate surface slope square with EW equation as the plant model. $q_{r^2}=0$, $q_{m^2}=1$ and $m^2_{set}=0.005$.

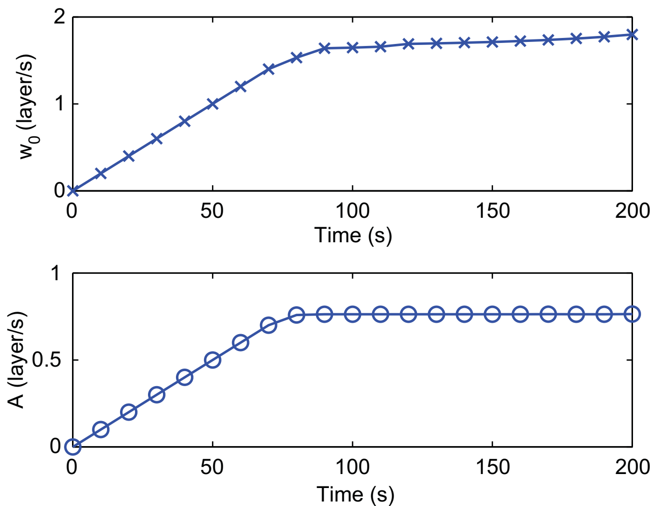

Fig. 20. Input profiles for aggregate slope-only control problem with EW equation as the plant model. $q_{r^2}=0$, $q_{m^2}=1$ and $m^2_{set}=0.005$.

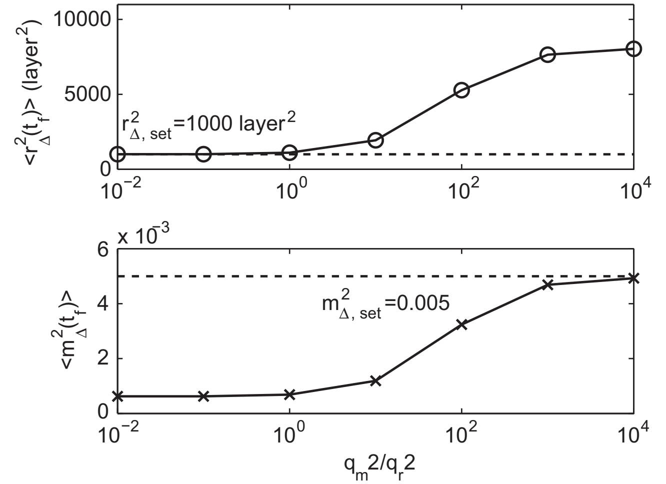

Fig. 21. $\langle r^2_{\Delta}(t_f)\rangle$ and $\langle m^2_{\Delta}(t_f)\rangle$ at the end of closed-loop simulations ($t=200$ s) for different penalty weighting factors in the predictive controller with EW equation as the plant model. $10^{-2}\le q_{m^2}\le 10^4$, $q_{r^2}=1$, $r^2_{set}=1000$ and $m^2_{set}=0.005$.

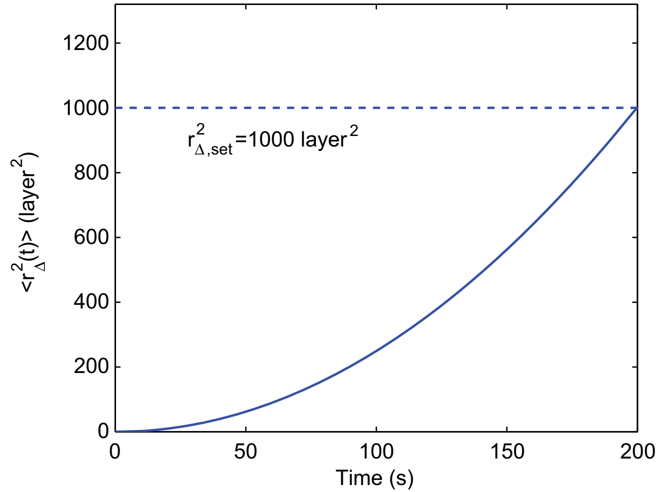

Fig. 22. Profile of expected aggregate surface roughness square with kMC model as the plant model. $q_{r^2}=1$, $q_{m^2}=0$ and $r^2_{set}=1000$.

5.2. MPC application to kMC model

In this subsection, the kMC model is used in the closed-loop control problem as the plant model, while all the other settings remain the same. Fig. 22 shows the aggregate surface roughness in the case of roughness-only control while Fig. 23 shows the aggregate surface slope in the case of slope-only control. From both plots, we see that both aggregate roughness and slope successfully reach their set-points at the end of the simulations (t_f=200 s). Furthermore, the closed-loop evolution profiles with kMC as the plant model are very similar to the closed-loop profiles that use the EW equation as the plant model, which implies that the EW equation model used in this work can accurately predict the kMC simulation results.

Simultaneous regulation of aggregate surface roughness and slope has also been investigated. Similar to the case where the EW equation is used as the plant model, the weighting factor of aggregate slope square, q_{r^2}, is kept at 1, and the weighting factor of aggregate roughness square, q_{m^2}, ranges from 10^{-2} to 10^4. Fig. 24 shows the values of expected aggregate roughness and slope at the end of simulations as a function of q_{m^2}/q_{r^2}. It can be seen that the expected value of aggregate roughness approaches its set-point as q_{m^2} increases at the cost of larger deviation of the aggregate slope from its set-point.

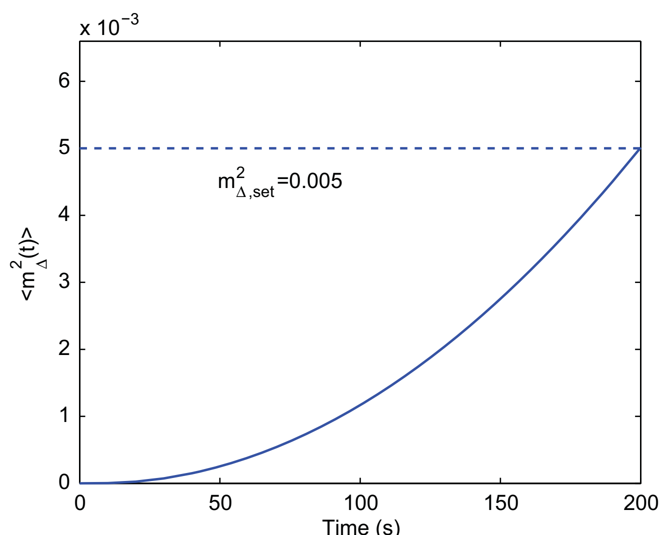

Fig. 23. Profile of expected aggregate surface slope square with kMC model as the plant model. $q_{r^2}=0$, $q_{m^2}=1$ and $m^2_{set}=0.005$.

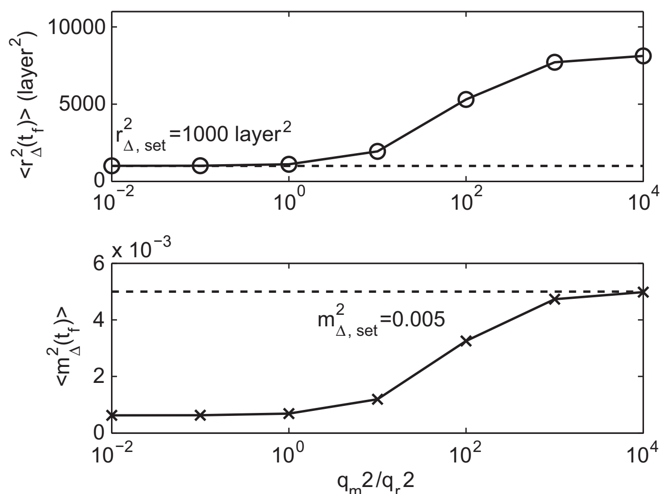

Fig. 24. $\langle r^2_\Delta(t_f)\rangle$ and $\langle m^2_\Delta(t_f)\rangle$ at the end of closed-loop simulations ($t=200$ s) for different penalty weighting factors in the predictive controller with kMC model as the plant model. $10^{-2}\le q_{m^2}\le 10^4$, $q_{r^2}=1$, $r^2_{set}=1000$ and $m^2_{set}=0.005$.

Though with the current actuator design it is difficult to reach the set-points of aggregate roughness and slope at the same time, the actuator design can be easily improved to reach this goal. For example, one way to do this is to introduce a spatially distributed deposition rate profile with multiple sine waves that have independently controlled magnitude values, and the mean deposition rate and the magnitude value of each sine wave are used as the manipulated variables in the control problem. In this way, set-points of both aggregate roughness and slope can be achieved simultaneously; for details on this approach, see Huang et al. (2012).

6. Conclusions

In this work, a two species thin film deposition process is simulated via a kinetic Monte–Carlo method in a large square lattice ($L=40{,}000$). Different growth mechanisms are used for each species (ZnO and Al) and a patterned deposition rate profile is introduced to generate significant aggregate surface roughness and slope at a length scale comparable to the wavelength of visible light. An Edwards–Wilkinson type equation for the aggregate surface profile is used to predict the surface temporal evolution of aggregate surface roughness and slope. A model predictive controller is designed to regulate aggregate surface roughness and slope to desired levels, and the controller is applied to the EW equation and the kMC model of the deposition process with $L=40{,}000$. Simulation results demonstrate the applicability and effectiveness of the controller and of the spatially patterned deposition rate profile. The results of this work pave the way for the manufacturing of TCO layers with desired light trapping properties.

Acknowledgment

Financial support from the National Science Foundation, CBET-0652131, and a UCLA Doctoral Dissertation Year Fellowship for Jianqiao Huang, are gratefully acknowledged.

References

Buzea, C., Robbie, K., 2005. State of the art in thin film thickness and deposition rate monitoring sensors. Rep. Prog. Phys. 68, 385–409.
Christofides, P.D., 2001. Nonlinear and Robust Control of PDE Systems: Methods and Applications to Transport-Reaction Processes. Birkhäuser, Boston.
Christofides, P.D., Armaou, A., Lou, Y., Varshney, A., 2008. Control and Optimization of Multiscale Process Systems. Birkhäuser, Boston.
Das, R., Jana, T., Ray, S., 2005. Degradation studies of transparent conducting oxide: a substrate for microcrystalline silicon thin film solar cells. Sol. Energy Mater. Sol. Cells 86, 207–216.
Edwards, S.F., Wilkinson, D.R., 1982. The surface statistics of a granular aggregate. Proc. R. Soc. London Ser. A Math. Phys. Eng. Sci. 381, 17–31.
Gillespie, D.T., 1976. A general method for numerically simulating the stochastic time evolution of coupled chemical reactions. J. Comput. Phys. 22, 403–434.
Gospodyn, J., Sit, J.C., 2006. Characterization of dielectric columnar thin films by variable angle mueller matrix and spectroscopic ellipsometry. Opt. Mater. 29, 318–325.
Green, M.A., 2007. Thin-film solar cells: review of materials, technologies and commercial status. J. Mater. Sci. Mater. Electron. 18, 15–19.
Hu, G., Huang, J., Orkoulas, G., Christofides, P.D., 2009a. Investigation of film surface roughness and porosity dependence on lattice size in a porous thin film deposition process. Phys. Rev. E 80, 041122.
Hu, G., Orkoulas, G., Christofides, P.D., 2009b. Modeling and control of film porosity in thin film deposition. Chem. Eng. Sci. 64, 3668–3682.
Huang, J., Hu, G., Orkoulas, G., Christofides, P., 2010. Dependence of film surface roughness and slope on surface migration and lattice size in thin film deposition processes. Chem. Eng. Sci. 65, 6101–6111.
Huang, J., Hu, G., Orkoulas, G., Christofides, P.D., 2011a. Dynamics and lattice-size dependence of surface mean slope in thin-film deposition. Ind. Eng. Chem. Res. 50, 1219–1230.
Huang, J., Zhang, X., Orkoulas, J., Christofides, P.D., 2011b. Dynamics and control of aggregate thin film surface morphology for improved light trapping: implementation on a large-lattice kinetic monte carlo model. Chem. Eng. Sci. 66, 5955–5967.
Huang, J., Orkoulas, G., Christofides, P.D., 2012. Simulation and control of aggregate surface morphology in a two-stage thin film deposition process for improved light trapping. Chem. Eng. Sci. 71, 520–530.
Isabella, O., Krč, J., Zeman, M., 2010. Modulated surface textures for enhanced light trapping in thin-film silicon solar cells. Appl. Phys. Lett. 97, 101106.
Krč, J., Zeman, M., 2003. Effect of surface roughness of ZnO: Al films on light scattering in hydrogenated amorphous silicon solar cells. Thin Solid Films 426, 296–304.
Lauritsen, K.B., Cuerno, R., Makse, H.A., 1996. Noisy Kuramote–Sivashinsky equation for an erosion model. Phys. Rev. E 54, 3577–3580.
Levine, S.W., Clancy, P., 2000. A simple model for the growth of polycrystalline Si using the kinetic Monte Carlo simulation. Model. Simul. Mater. Sci. Eng. 8, 751–762.
Levine, S.W., Engstrom, J.R., Clancy, P., 1998. A kinetic Monte Carlo study of the growth of Si on Si(100) at varying angles of incident deposition. Surf. Sci. 401, 112–123.
Mirica, E., Kowach, G., Evans, P., Du, H., 2004. Morphological evolution of ZnO thin films deposited by reactive sputtering. Cryst. Growth Des. 4, 147–156.
Moller, S., Palumbo, R., 2001. Solar thermal decomposition kinetics of ZnO in the temperature range 1950–2400 k. Chem. Eng. Sci. 56, 4505–4515.
Muller, J., Rech, B., 2004. TCO and light trapping in silicon thin film solar cells. Sol. Energy 77, 917–930.
Ni, D., Christofides, P.D., 2005. Multivariable predictive control of thin film deposition using a stochastic PDE model. Ind. Eng. Chem. Res. 44, 2416–2427.
Poruba, A., Fejfar, A., Remeš, Z., Špringer, J., Vaněček, M., Kočka, J., 2000. Optical absorption and light scattering in microcrystalline silicon thin films and solar cells. J. Appl. Phys. 88, 148–160.

Reese, J.S., Raimondeau, S., Vlachos, D.G., 2001. Monte Carlo algorithms for complex surface reaction mechanisms: efficiency and accuracy. J. Comput. Phys. 173, 302–321.
Rowlands, S.F., Livingstone, J., Lund, C.P., 2004. Optical modelling of thin film solar cells with textured interface using the effective medium approximation. Sol. Energy 76, 301–307.
van Sark, W., Brandsen, G.W., Fleuster, M., Hekkert, M.P., 2007. Analysis of the silicon market: will thin films profit. Energy Policy 35, 3121–3125.
Varshney, A., Armaou, A., 2005. Multiscale optimization using hybrid PDE/kMC process systems with application to thin film growth. Chem. Eng. Sci. 60, 6780–6794.
Varshney, A., Armaou, A., 2006. Optimal operation of GaN thin-film epitaxy employing control vector parametrization. AIChE J. 52, 1378–1391.
Vvedensky, D.D., Zangwill, A., Luse, C.N., Wilby, M.R., 1993. Stochastic equations of motion for epitaxial growth. Phys. Rev. E 48, 852–862.
Wächter, A., Biegler, L.T., 2006. On the implementation of an interior-point filter line-search algorithm for large-scale nonlinear programming. Math. Programming 106 (1), 25–57.
Wang, L., Clancy, P., 2001. Kinetic Monte Carlo simulation of the growth of polycrystalline Cu films. Surf. Sci. 473, 25–38.
Yang, Y.G., Johnson, R.A., Wadley, H.N., 1997. A Monte Carlo simulation of the physical vapor deposition of nickel. Acta Mater. 45, 1455–1468.
Zeman, M., Vanswaaij, R., 2000. Optical modeling of α-Si : H solar cells with rough interfaces: effect of back contact and interface roughness. J. Appl. Phys. 88, 6436–6443.
Zhang, X., Huang, J., Orkoulas, G., Christofides, P.D., 2012. Controlling aggregate thin film surface morphology for improved light trapping using a patterned deposition rate profile. Chem. Eng. Sci. 67, 101–110.